



Effect of Width-Thickness and Depth-Thickness on the Cyclic Flexural Buckling Behavior of Hollow Structural Sections

M. Fadden¹, J. McCormick²

Abstract

HSS members are desirable for structural applications due to their flexural, compression, and torsional resistance. To allow for increased utilization of hollow structural sections (HSS) in cyclic bending applications, their cyclic flexural stability and local buckling behavior under large rotations must be understood. Experimental tests of HSS with width-thickness (b/t) and depth-thickness (h/t) ratios of 8.46 to 31.3 and 19.9 to 48.5, respectively, show their suitability for cyclic bending applications provided b/t and h/t are limited. The effect of the b/t and h/t ratios are found to be interdependent and correlate with the occurrence of local buckling and loss of moment capacity with cycling to increased deformation levels. In order to better understand the behavior of HSS beam members under cyclic loads, a finite element model (FEM) that accounts for localized material properties and local buckling behavior is developed and correlated to experimental results. Geometric perturbations of the section geometry are introduced based on an eigenvalue buckling analysis to approximate observed experimental local buckling behavior. From the correlated model, 133 sections are analyzed, with the section sizes spanning from HSS 152.4x50.8x4.8 to HSS 508.0x304.8x15.9, allowing a wide range of b/t and h/t ratios to be considered. The results confirm the interdependence of b/t and h/t on the local buckling behavior and provide a basis for defining limiting values to prevent local buckling and subsequent loss of moment capacity under cyclic bending loads.

1. Introduction

Hollow structural sections (HSS) are used in a number of building applications because of their favorable bending, compression, and torsional resistance. Applications of HSS include use as column members, bracing elements, truss elements, exposed structural steel, and cladding supports. However, the use of HSS in seismic moment resisting frames has been limited to HSS columns or concrete filled tubes (CFT) columns connected to wide flange beams (Hajjar 2000, Kurobane 2002, Packer 2000, Nishiyama and Morino 2004). Tube-based seismic moment resisting frames with HSS-to-HSS moment connections have potential to reduce the seismic weight of a structure, limit lateral bracing requirements, and open a new application for HSS. To be able to utilize HSS beam members, it is important to fully understand the local buckling behavior and subsequent degradation of moment capacity due to cycling and increasing rotation

¹ Graduate Student Research Assistant, University of Michigan <fadden@umich.edu>

² Assistant Professor, University of Michigan, <jpmccorm@umich.edu>

levels. Excessive local buckling can lead to unstable plastic hinges and premature failure of the beam member.

1.1 Background

Several previous studies have considered the bending behavior of HSS under monotonically increasing loads. The results from experimental studies suggest that the width-thickness (b/t) and depth-thickness (h/t) ratios control the local buckling behavior and moment capacity of HSS beam members (Korol and Houdba 1972, Hasan and Hancock 1988, Wilkinson and Hancock 1998). To further the use of HSS in seismic applications, recent large-scale experimental testing of HSS beam members has considered their behavior under cyclic bending loads (Brescia et al. 2010, Fadden and McCormick 2011). The cyclic testing results reiterate the importance of b/t and h/t observed during monotonic testing and provide a better understanding of the expected cyclic local buckling behavior.

Analytical models have been developed to both predict the behavior and understand the different failure modes of HSS members. Sohal and Chen (1988) considered the local buckling behavior of round HSS columns and developed a kinematic model that can be utilized to predict the cyclic behavior based on several assumptions including the critical strain, shape and propagation of the buckle, and stress in the HSS member. Key et al. (1988) developed a theoretical plastic mechanism model to predict the post-peak load-deflection behavior. This yield line model, based on the buckled shape, is composed of three components: plate folding, corner yielding, and folding corner restraint mechanisms.

More recent studies have utilized finite element models (FEM). Nakashima and Liu (2005) used FEM to study HSS columns under different axial load ratios to failure. This study captured the local buckling behavior and noted the importance of the magnitude of the axial load and its effect on the hysteretic behavior. Goto et al. (1998) modeled large HSS columns using a three-surface cyclic metal plasticity model which can provide very accurate results when calibrated to experimental data. Other models of HSS consider their use as CFT columns under cyclic loads. These models utilize fiber elements that have constitutive relationships for both the concrete and steel. The model also accounts for confinement of the concrete core and cyclic local buckling of the steel tube (Denavit et al. 2010). Finite element analyses of square and rectangular HSS beam sections are limited and have focused on sections under monotonic bending loads (Wilkinson and Hancock 2002). This model utilized imperfections of the geometry to produce buckling behavior and load-displacement results similar to those observed in experimental testing. The results from this model reiterate the importance of the b/t and h/t ratios on the local buckling behavior.

1.2 Objective

The experimental testing and analytical study described in this paper addresses the limited cyclic testing and finite element modeling of square and rectangular HSS beam members under cyclic bending loads. This study considers the local buckling behavior observed during experimental testing and correlates the buckling to the b/t and h/t ratios by noting their effect on the hysteretic behavior. A FEM is calibrated to eleven experimentally tested HSS beam members by minimizing the difference in maximum moments between the model and the experimental results. The model utilizes experimentally measured material properties and geometric

imperfections of the section geometry to obtain the desired local buckling and hysteretic behavior. The validated model is then extrapolated to 133 different HSS beam members. The parametric study considers the effect of geometric properties on the local buckling behavior by correlating the effect of the b/t and h/t ratios on the hysteretic behavior and decrease in cyclic maximum moment with continued cycling. Plots of the degradation behavior versus the b/t and h/t ratios provide insight into the interdependence of the geometric properties on the local buckling and hysteretic behavior of HSS members undergoing cyclic bending.

2. Experimental Test Program

The experimental test program examines the cyclic hysteretic behavior of eleven full-scale square and rectangular HSS beams. These tests consider the ability of HSS beams members to develop appropriate plastic hinge behavior, ductility, energy dissipation and limited local buckling consistent with strong column-weak beam moment frame design requirements. Further details in regards to this study can be found in Fadden and McCormick (2011).

2.1 HSS Experimental Specimens

Eleven standard US cold-formed HSS specimens are considered with sizes similar to those that could be used in low-rise HSS moment frame systems. The depth of the sections ranges from 203.2 mm to 304.8 mm, while the width of the sections ranges from 101.6 mm to 203.2 mm. The wall thickness is either 6.4 mm or 9.5 mm. The sections are listed in Table 1 with their associated properties. The b/t ratio ranges from 8.46 to 31.3 and the h/t ratio ranges from 19.9 to 48.5. These values cover a significant portion of the width-thickness and depth-thickness ratios available in the US market and will allow for determination of the b/t and h/t ratios which lead to premature local buckling under increasing cyclic rotations. The HSS specimens are manufactured using standard ASTM A500 Gr. B steel with a minimum specified tensile yield stress, F_y , of 317 MPa, and a minimum specified ultimate tensile strength, F_u , of 400 MPa. The theoretical minimum plastic moment capacity, $(M_p)_{min}$, for each section is listed in Table 1 and is calculated using $(M_p)_{min} = Z_x F_y$ assuming F_y equals the minimum specified tensile yield strength.

Table 1. Experimental HSS specimens and properties

Section	Wall thickness	Area	Width- thickness ratio	Depth- thickness ratio	Plastic section modulus	Minimum plastic moment capacity
(mm x mm x mm)	t (mm)	A (mm ²)	(b/t)	(h/t)	Z (cm ³)	$(M_p)_{min}$ (kN-m)
HSS 203.2x101.6x6.4	5.66	3380	14.2	31.3	218	69.1
HSS 203.2x101.6x9.5	8.86	4889	8.46	19.9	308	97.7
HSS 203.2x152.4x6.4	5.66	3980	22.8	31.3	277	87.8
HSS 203.2x152.4x9.5	8.86	5786	14.2	19.9	395	125.3
HSS 203.2x203.2x6.4	5.66	4580	31.3	31.3	336	106.6
HSS 203.2x203.2x9.5	8.86	6708	19.9	19.9	482	152.8
HSS 254.0x101.6x6.4	5.66	3980	14.2	39.9	312	98.8
HSS 254.0x152.4x6.4	5.66	4580	22.8	39.9	387	122.7
HSS 254.0x203.2x6.4	5.66	5179	31.3	39.9	461	146.1
HSS 304.8x101.6x6.4	5.66	4580	14.2	48.5	420	133.1
HSS 304.8x152.4x6.4	5.66	5179	22.8	48.5	510	161.7

2.2 Experimental Test Setup

The experimental test setup (Figure 1) used to study the cyclic bending behavior of HSS consists of a load frame, actuator, HSS beam member, and instrumentation. The HSS beam member is cantilevered vertically within the test frame and is loaded in displacement control through a pin connection at the top. The fixed end of the HSS is sandwiched between two large angles with added stiffener plates to provide a reusable connection and ensure that the inelastic deformation occurs within the HSS and not in the connection. The connection is not designed to be a practical connection for moment frame systems. Four strain gages are attached on each flange at 76.2 mm, 228.6 mm, 457.2 mm and 914.4 mm from the fixed connection. A grid of infrared optical tracking markers is arranged on the web to measure displacements and rotations of the member in the plastic hinge region. A 600 kN load cell attached to the actuator measures the applied load, while an optical tracking marker is placed on the loading pin to measure the displacement at the end of the HSS beam. The loading protocol, run in displacement control at a quasi-static loading rate, consists of increasing end displacements to simulate a farfield-type ground motion and provide a means of evaluating the moment-rotation behavior of HSS under large cyclic deformations. The test setup allows for a pin displacement of 254 mm, which equates to a maximum rotation of 0.08 radians.

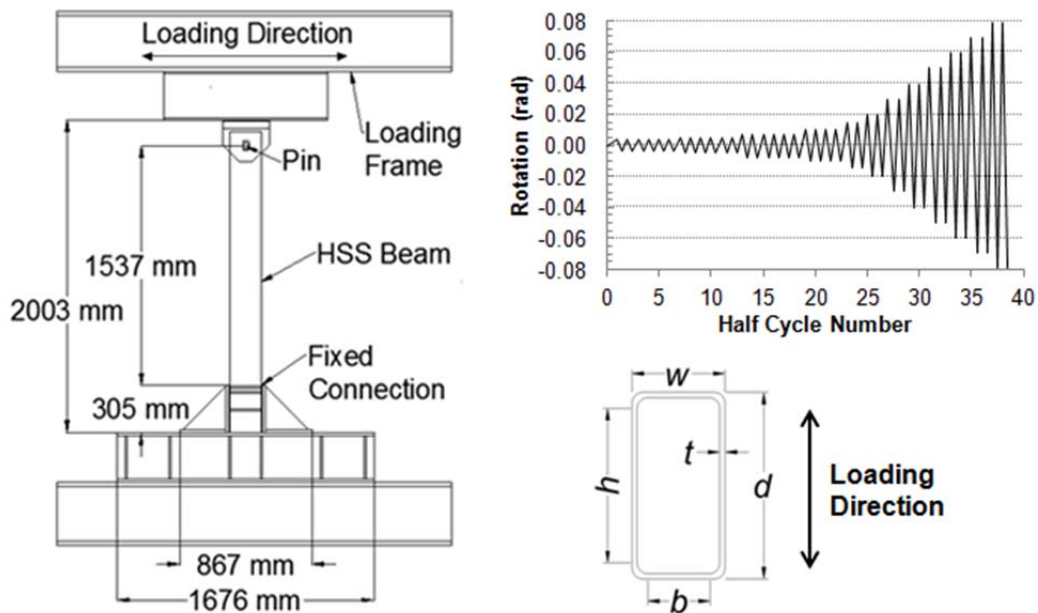


Figure 1: Experimental test setup and loading protocol

2.2 Hysteretic Behavior

Each moment-rotation hysteresis curve is considered to understand the effects of local buckling on the development of stable plastic hinge behavior. Due to the presence of rigid rotation, many specimens did not reach the maximum rotation of 0.08 rad., but all reached at least 0.05 rad. The largest overall maximum moment, M_{max} , is 227.7 kN-m for the HSS 203.2x203.2x9.5 and the smallest M_{max} is 90.0 kN-m for the HSS 203.2x101.6x6.4. The rotation at which the maximum moment is reached and local buckling initiates spanned between 0.017 rad. for the HSS 254.0x203.2x6.4 and 0.035 rad. for the HSS 203.2x152.4x9.5. Analysis of the results indicates that members with low b/t and h/t ratios tend to maintain their moment capacity to higher

rotation levels without considerable degradation, longer than sections with high b/t and h/t ratios. All sections reach a moment capacity greater than the theoretical minimum plastic moment capacity, $(M_p)_{min}$. The HSS 254.0x203.2x6.4 has the lowest $M_{max}/(M_p)_{min}$ of 1.23 and the HSS 203.2x203.2x101.6x9.5 has the highest $M_{max}/(M_p)_{min}$ of 1.71. These results imply that all sections will reach their theoretical minimum plastic moment capacity prior to excessive local buckling.

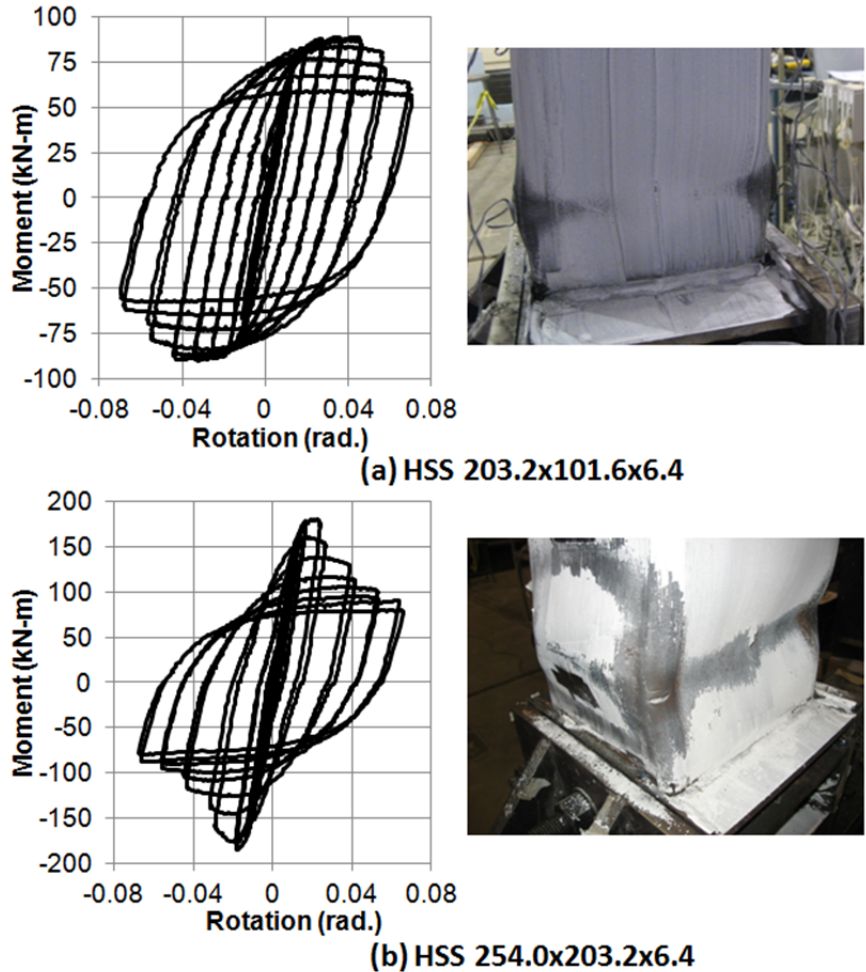


Figure 2. Moment-rotation hysteresis plots and photographs of the experimental HSS beam members at the end of cycling: (a) HSS 203.2x101.6x6.4 and (b) HSS 254.0x203.2x6.4

Figure 2 depicts the change in shape of the hysteresis plots due to varying amounts of localized buckling for the HSS 203.2x101.6x6.4 ($b/t=14.2$, $h/t=31.3$) and the HSS 254.0x203.2x6.4 ($b/t=31.3$, $h/t=39.9$). The HSS 203.2x101.6x6.4 (Figure 2a) has a full hysteretic curve with only a moderate decrease in moment capacity at large rotation levels. It reaches M_{max} of 90.0 kN-m at 0.027 rad., which it maintains with continued cycling up to nearly 0.046 rad. and then decreases to 54.6 kN-m during the 0.071 rad. cycle. The HSS 254.0x203.2x6.4 (Figure 2b) reaches M_{max} of 185.0 kN-m at 0.018 rad. and quickly degrades to 76.5 kN-m during the 0.068 rad. cycle. For the HSS 254.0x203.2x6.4, the low rotation level at which the maximum moment is reached can be attributed to the high section stiffness compared to the HSS 203.2x101.6x6.4. In addition, the inability of the HSS 254.0x203.2x6.4 to maintain M_{max} with continued cycling can be attributed to large amounts of local buckling corresponding to its high b/t and h/t ratios. Visual inspection

of each section is consistent with the hysteretic moment-rotation behavior. There is only moderate local buckling in the flanges and minor buckling in the webs of the HSS 203.2x101.6x6.4 (Figure 2a). Conversely, the HSS 254.0x203.2x6.4 shows large amounts of local buckling in both the flanges and webs, which leads to tearing at the corners in later cycles at high rotation levels (Figure 2b). Based on these results, it is clear that higher b/t and h/t ratios lead to increased buckling and degradation of the maximum cyclic moment at increased rotation levels (Fadden and McCormick 2011).

3. Finite Element Model Development and Calibration

To address the limited experimental results, a FEM is developed that allows for the prediction of the cyclic hysteretic bending behavior of HSS. The model is calibrated to the eleven experimental sections and subjected to the displacement protocol observed during experimental testing. To achieve accurate hysteretic behavior, the model utilizes standard section geometry, experimentally measured material properties, and geometric imperfections of the mesh based on an eigenvalue buckling analysis.

3.1 Finite Element Model

Abaqus FEA (Version 6.8-1) (DSS 2008) is used to model the cyclic bending behavior of HSS beam members. Like the experimental tests, the model simulates a fixed-end cantilever beam. One end is displaced vertically and the other end is constrained from moving. The HSS cross-section is the same as shown in Figure 1 and uses the section geometry reported in the AISC Manual (AISC 2010). The corner radius is assumed to be twice the wall thickness of the modeled section. The model mesh (Figure 3) is divided into three regions: the fixed end region, extending 30.5 cm from the fixed end; the 2.5 cm transition region; and the displaced end region, which includes the rest of the member. The mesh is optimized through a convergence study where the displaced end region uses 5.0 cm square elements and the fixed end region uses 1.3 cm square elements. In these regions, 4-node double curved thin or thick shell element with reduced integration, and hourglass control are utilized. The transition region utilizes a 3-node general-purpose shell element that considers finite membrane strains.

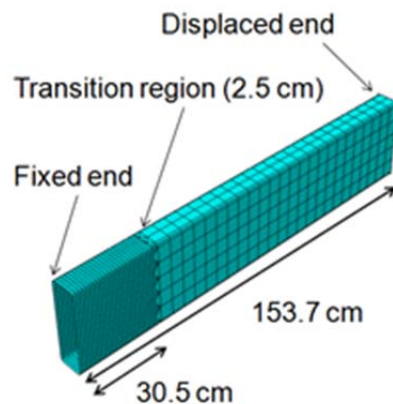


Figure 3. Mesh regions and geometry of the HSS FEM

3.2 Material Properties

To consider the variability of material behavior across the cross-section, ten coupon specimens are taken from various locations around the perimeter of the HSS 203.2x203.2x6.4 and HSS

203.2x152.4x9.5 members. The findings from these tensile coupon tests help to better understand the effects of cold working on the corners of the section and the heat affected zone near the weld seam. ASTM A370 (2011) and E8 (2009) are followed to carry out the tensile coupon tests. However, limits due to the HSS geometry, particularly at the corners, do not allow for strict adherence to the standards.

Figure 4 provides stress-strain curves for four different coupon specimen locations on the HSS 203.2x203.2x6.4 and HSS 203.2x152.4x9.5. For both sections, locations (i) and (iv) refer to the corner and weld seam, respectively, and locations (ii) and (iii) refer to the flats. It is evident from the results that the cold worked region, the weld material, and the heat affected zone lead to vastly different material properties than those observed for the flats of the section. The corner and weld specimens have higher yield and ultimate strength values and low ductility. Coupon specimens obtained from the flats show lower yield and ultimate strength values, but higher amounts of ductility. Variations in tensile material properties at different locations along the flats tend to be very small. Table 2 provides the yield and ultimate strength for the four different locations of the two HSS members. The highest yield stress, F_y , measured using the 0.2% offset yield method is 619.5 MPa from the weld coupon specimen (iv) taken from the HSS 203.2x152.4x9.5, while the lowest measured yield stress is 417.7 MPa for the coupon specimen taken from the short side flat (ii) of the HSS 203.2x152.4x9.5. The highest ultimate strength is 661 MPa measured from the coupon specimen at the weld (iv) of the HSS 203.2x152.4x9.5, while the lowest measured ultimate strength is 495.8 MPa from the coupon specimen taken from the short side flat (ii) of the HSS 203.2x152.4x9.5.

In the finite element model only material properties for the corner (i) and flat (ii) are used for each section. The weld (iv) material property is ignored in each section because it represents a relatively small area. Specimens that are 8.0 mm thick or less use material properties from the HSS 203.2x203.2x6.4 with F_y of 452.0 MPa and F_u of 520.5 MPa for the flats and F_y of 560.0 MPa and F_u of 612.1 MPa for the corners. Likewise, specimens that are 9.5 mm thick or greater use material properties from the HSS 203.2x152.4x9.5 with F_y of 418 MPa and F_u of 496 MPa for the flats and F_y of 526 MPa and F_u of 582 MPa for the corners. The material models use a kinematic hardening law and do not account for strain rate effects.

Table 2. Experimental HSS Material Properties

Section (mm x mm x mm)	Yield Stress	Ultimate Stress
	F_y (MPa)	F_u (MPa)
HSS 203.2x203.2x6.4		
(i) corner	560.0	612.1
(ii) flat	452.0	520.5
(iii) flat (near weld)	476.0	545.8
(iv) weld	432.3	606.8
HSS 203.2x152.4x9.5		
(i) corner	526.1	582.4
(ii) flat (short side)	417.7	495.8
(iii) flat (long side)	458.2	516.8
(iv) weld	619.5	661.4

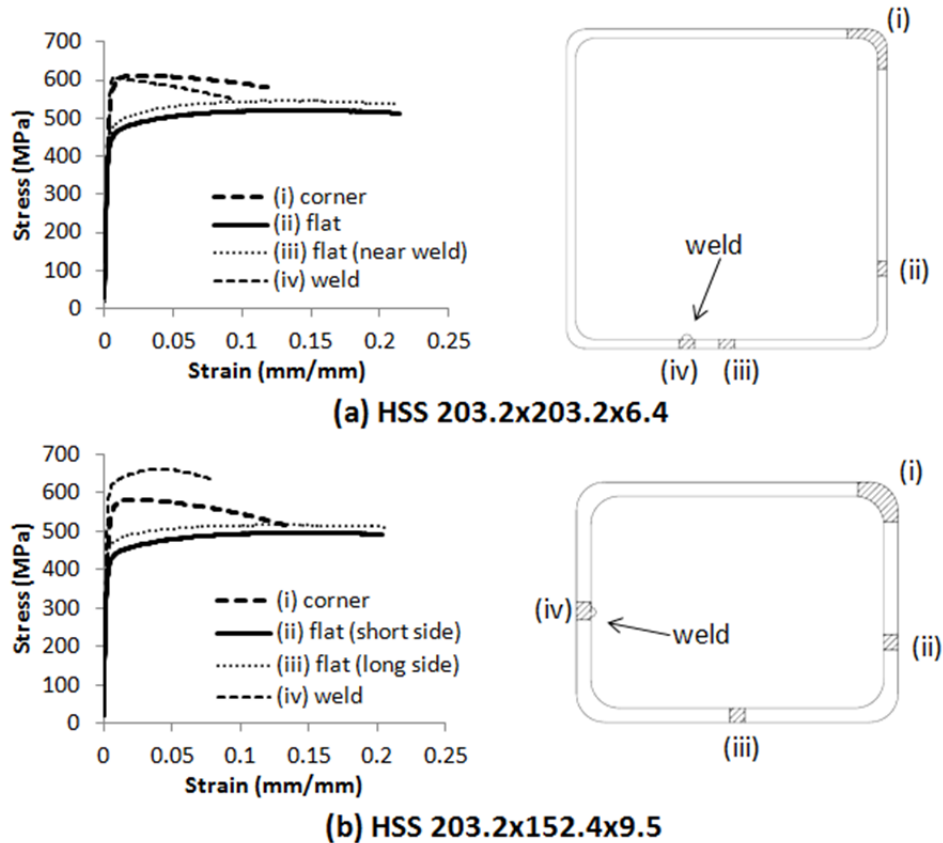


Figure 4. Tensile coupon test results for various locations along the cross section of the (a) HSS 203.2x101.6x6.4 and (b) HSS 203.2x152.4x9.5.

3.3 Geometric Imperfections

To produce an accurate finite element model for HSS beam members, the local buckling behavior must be captured. To capture local buckling and hysteretic behavior consistent with experimental findings a geometric imperfection is added to each HSS beam member to create a continuous buckling problem. This removes the buckling bifurcation and ensures buckling in the desired mode. These perturbations or imperfections to the geometry are based on mode shapes from an eigenvalue buckling analysis. The perturbations are a superposition of two different eigenmodes which achieve a buckled shape similar to that observed during experimental cyclic bending tests of HSS. The amount of geometric imperfection is optimized to provide a procedure for further parametric studies on specimens without experimental data. The eigenvalue buckling analysis produces the shape of the perturbation with a maximum nodal value of unity. This value is scaled to the desired value to produce accurate results. The models of each previously experimentally tested section are run with no imperfection and maximum imperfections of 2.54 mm, 5.08 mm, 7.62 mm, and 10.16 mm, to determine which value provides the most accurate correlation. The calibration of the FEM aims to minimize the error between the overall maximum moment measured experimentally and that obtained from the finite element analysis. Additionally, the hysteretic behavior should be similar throughout the loading protocol including the stiffness and degradation of the moment capacity with continued cycling.

The percent error between the experimental and finite element analysis' overall maximum moment for different imperfection magnitudes is provided in Figure 5. For seven of the eleven

section sizes, the model over predicts the maximum moment observed. With zero imperfection, the model of the HSS 203.2x101.6x6.4 over predicts M_{max} by 22% compared to the experimental results providing the greatest difference of any section. The model of the HSS 203.2x203.2x9.5 under predicts the experimental M_{max} by 2% at zero imperfection, providing the smallest difference of any section. Increasing the magnitude of the imperfection, decreases the M_{max} for each section and increases the ease at which the section begins to buckle locally before fully developing its plastic hinge. Specimens with $b/t \leq 14.2$ and $h/t \leq 19.9$ tend to show a large under prediction of the experimental M_{max} at zero imperfection. For example, the HSS 203.2x101.6x9.5 and HSS 203.2x152.4x9.5 under predicts M_{max} by 9% and 7% respectively, at zero imperfection.

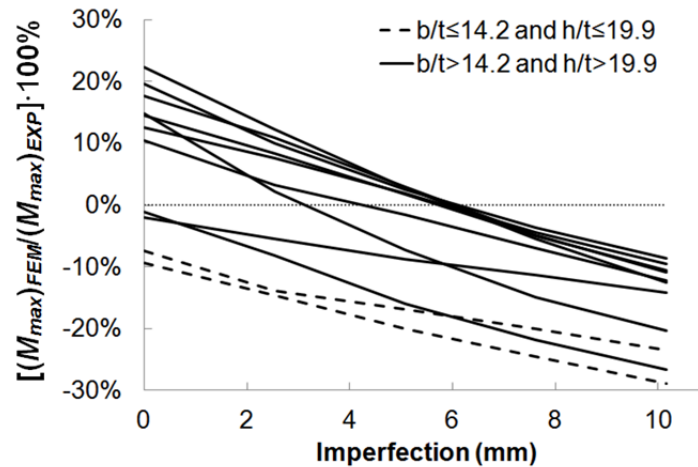


Figure 5. Percent error between the maximum moment of the FEM and the experimental maximum moment

In order to determine a procedure to accurately capture local buckling, a magnitude for the imperfection is chosen which minimizes the average percent error for the eleven sections. The average percent error for M_{max} is minimized to 5% with a 5.1 mm maximum imperfection. When sections with $b/t \leq 14.2$ and $h/t \leq 19.9$ are considered with no imperfection, the average error is further reduced to 2% with a 5.1 mm maximum imperfection for all other sections. The sections with $b/t \leq 14.2$ and $h/t \leq 19.9$, which are highlighted by dashed lines, are very compact and show minimal buckling during experimental testing suggesting that the use of no imperfection for low b/t and h/t ratios is justified. Thus, the calibrated finite element model employs the following rule, when $b/t > 14.2$ and $h/t > 19.9$, a maximum imperfection of 5.1 mm is used while all other sections with $b/t \leq 14.2$ and $h/t \leq 19.9$ use no imperfection.

3.4 Comparison of Experimental and FEM Hysteretic Behavior

The hysteresis curves from the experimental tests of the eleven sections are compared to the finite element analysis results. The largest M_{max} from the finite element analysis is 207.7 kN-m for the HSS 203.2x203.2x9.5 and the smallest M_{max} is 92.5 kN-m for the HSS 203.2x101.6x6.4. These sizes correspond to the same sections where the maximum moments are observed during experimental testing. The rotation at which the maximum moment is reached and local buckling initiates spans between 0.015 rad. for the HSS 304.8x152.6x6.4 and 0.033 rad. for the HSS 203.2x101.6x9.5. Each section reaches a moment capacity greater than the theoretical minimum plastic moment capacity, $(M_p)_{min}$. These results imply that all modeled experimental sections will also reach their plastic moment capacity without excessive local buckling.

Figure 6 compares the moment-rotation hysteresis plots from the finite element analysis and experimental results for the HSS 203.2x101.6x6.4 and the HSS 254.0x203.2x6.4. The calibrated model shows a very good correlation to the experimental data for both of these specimens. The maximum moment is well predicted and only differs by 3% and 2% for the HSS 203.2x101.6x6.4 and the HSS 254.0x203.2x6.4, respectively. The HSS 203.2x101.6x6.4 again has a full hysteric curve with only a moderate decrease in the moment capacity at large rotation levels and reaches M_{max} of 92.5 kN-m at 0.027 rad. then degrades steadily to 57.8 kN-m at 0.071 rad. The HSS 254.0x203.2x6.4 reaches M_{max} of 188.3 kN-m at 0.017 rad. and quickly degrades to 91.2 kN-m at 0.068 rad. All eleven specimens show a similar correlation between the experimental results and finite element analysis findings.

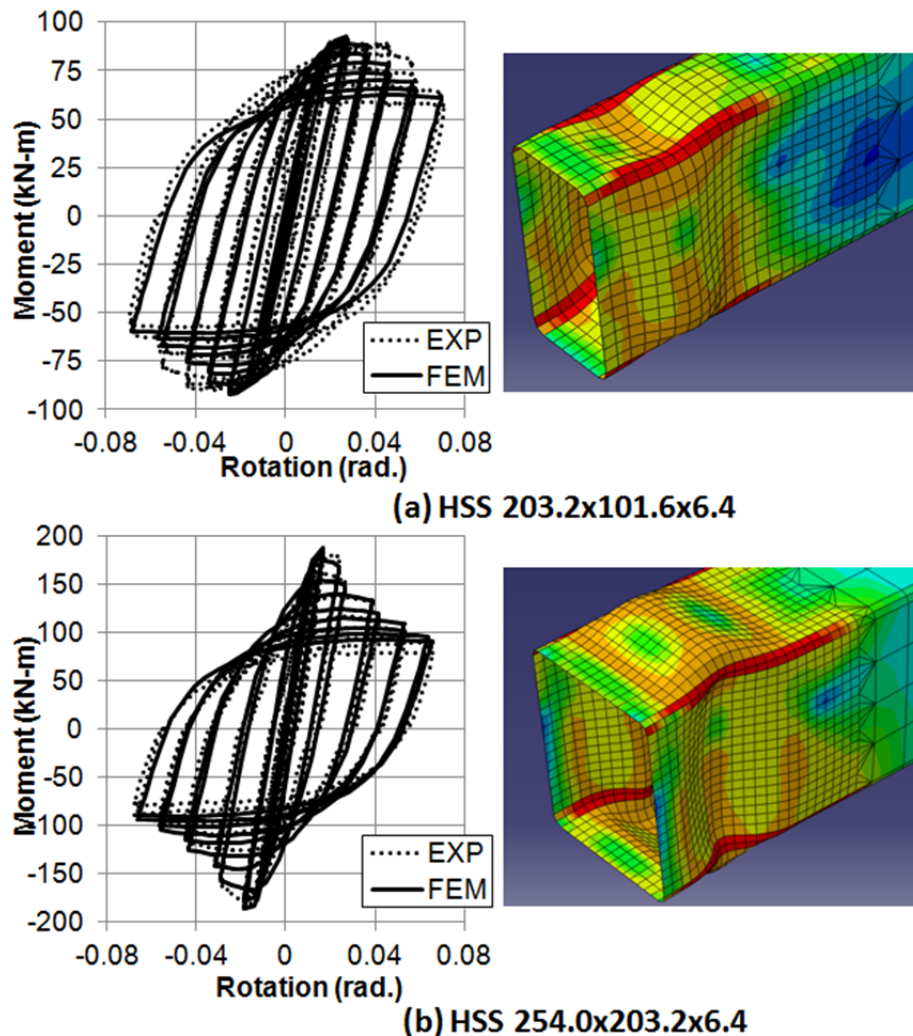


Figure 6. Moment-rotation hysteresis and of FEM the HSS beam members: (a) HSS 203.2x101.6x6.4 and (b) HSS 254.0x203.2x6.4

The inability of the HSS 254.0x203.2x6.4 to maintain M_{max} can be attributed to large amounts of local buckling corresponding to high b/t and h/t ratios. In the case of the finite element analysis of the HSS 203.2x101.6x6.4, the smaller decrease in moment capacity with continued cycling

can be attributed to lower b/t and h/t ratios. However, for the finite element results the degradation begins earlier in the loading protocol and degrades steadily to the final cycle. Visual inspection of the local buckling shown in the model is consistent with the observed hysteretic behavior. For the HSS 203.2x101.6x6.4 the local buckling is more pronounced in the webs than observed experimentally (Figure 6a). The HSS 254.0x203.2x6.4 buckled shape shows very good correlation with the experimental specimen (Figure 6b). The maximum moment for the final cycle from the finite element analysis of the HSS 254.0x203.2x6.4 is 14.7 kN-m higher than the experimental final cycle maximum moment and may be attributed to the lack of modeling of the tearing in the corners at later cycles which was observed experimentally. Based on these comparisons, it is shown that the calibrated FEM provides a relatively good match to the experimental data in terms of moment capacity, moment degradation, and local buckling behavior.

3.5 Cyclic Moment Degradation and Rotational Capacity

The hysteretic behavior observed experimentally and in the finite element analysis suggests that the amount of buckling is highly dependent on the b/t and h/t ratios. Past studies have also suggested that the effect of the b/t and h/t ratios are interdependent (Wilkinson and Hancock 1998). Figure 7 shows contour plots from a multiple linear regression analysis of the experimental data and finite element analysis results for the eleven experimental specimens. The effect of the b/t and h/t ratio can be quantified by considering the degradation of moment capacity from the overall M_{max} and the moment measured at the peak of the 0.04 rad. cycle. The 0.04 rad. rotation level is chosen because it will produce a rotation in the beam member greater than an interstory drift of 0.04 rad. which must be sustained by seismic moment connections (AISC 2006). The contour lines represent the percent degradation (in decimal form) of M_{max} at the 0.04 rad. rotation cycle with respect to the b/t and h/t ratio. The HSS 203.2x101.6x9.5 is included in the analysis, but omitted from the plots because its degradation is below 5%.

Comparing both the experimental (Figure 7a) and finite element analysis (Figure 7b) results, the FEM does an adequate job in capturing the general shape of the contours. The finite element results slightly over predict the amount of degradation at 0.04 rad. This is especially true at low b/t and h/t ratios. For example, at a b/t of 14.2 and h/t of 31.3, the finite element analysis predicts a moment degradation of about 12.5% of M_{max} , while the experimental results only show a moment degradation of about 5% of M_{max} at 0.04 rad. This phenomenon is probably due to an increase in local buckling seen in the webs of many of the modeled sections at intermediate rotation levels.

It is also useful to consider the rotation at which a percentage of M_{max} is preserved such that stability of the plastic hinge and section ductility is maintained with limited local buckling. Earthquake resistant design of moment frames systems requires that strong column-weak beam behavior is maintained throughout loading. This study considers the rotation level when 80% of M_{max} is reached, a typical limit attributed to a reduction in moment capacity in seismic design (AISC 2006). This limit can then be extended to inter-story drift capacity in actual design. Figure 7 compares the rotational capacity at 80% of M_{max} with respect to the b/t and h/t ratios for the experimental and finite element analysis results. The HSS 203.2x101.6x9.5, HSS 203.2x152.4x9.5 and, HSS 203.2x203.2x9.5 are excluded from the calculations and plots because they experience stable behavior and do not degrade below $0.8M_{max}$ throughout the

loading protocol. This can be attributed to their low b/t and h/t ratios. The slopes of the contour plots from the FEM results tend to be shallower, especially at b/t and h/t ratios less than 25 and 40, respectively. The failure rotations tend to be reasonably conservative, deviating by no more 0.008 rad. at $h/t \geq 45$. Overall, the contours plots produced from the finite element analysis results provide a good prediction of the experimental results. This suggests that the model is suitable for extrapolation to other sections.

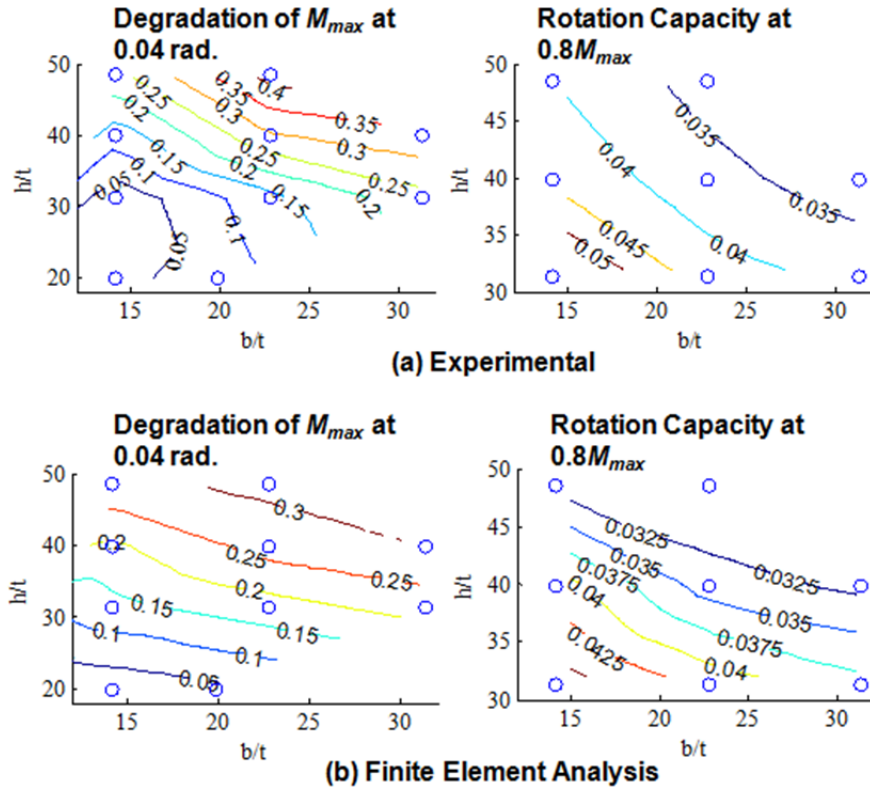


Figure 7. Degradation of M_{max} at 0.04 rad. and rotational capacity at $0.8M_{max}$ with respect to the b/t and h/t ratio for (a) Experimental and (b) Finite element analysis results.

4. Parametric Study

A parametric study is undertaken to consider the effect of b/t and h/t on the buckling and cyclic hysteretic HSS bending behavior. This study utilizes the previously calibrated HSS finite element model and expands the analysis to 133 different HSS sections, allowing the effect of local buckling on the degradation of the maximum moment and rotational capacity to be investigated. From this study, equations for estimating the post peak behavior of HSS under cyclic bending are extrapolated.

4.1 Parametric Study Details

The parametric study considers section sizes between HSS 152.4x50.8x4.8 and HSS 508.0x304.8x15.9, providing a large set of sections and a wide range of sizes and thicknesses. Specifically, the depths, d , range from 129 mm to 508 mm, the widths, w , range from 50.8 mm to 356 mm, and the thicknesses, t , range from 4.8 mm to 15.9 mm. Figure 8 shows the distribution of the parametric study specimens with respect to their b/t and h/t ratios. The limits for the specimens which have been tested experimentally is given by the rectangle. The width-thickness

and depth-thickness ratios considered in the parametric study fall near or within the range studied during experimental testing. The b/t ratio ranges from 7.0 to 31.5 and the h/t ratio ranges from 16.4 to 52.0. The wide range of sections permits consideration of the effect of local buckling on the degradation of the M_{max} and an understanding of the parameters that limit stable plastic hinge formation such as the b/t and h/t ratio.

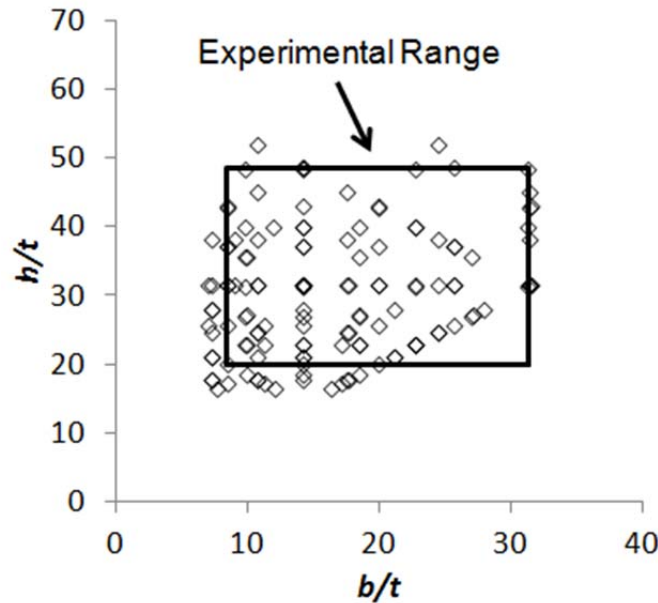


Figure 8. 133 parametric study specimens with respect to b/t and h/t ratios.

4.2 Parametric Study Moment Degradation and Rotational Capacity

To better understand the effect of local buckling, the degradation of M_{max} at 0.04 rad. and the rotation capacity at $0.8M_{max}$ is again considered. Figure 9 shows the effect of both the b/t and h/t ratios on the moment degradation and rotational capacity for the 133 modeled parametric study specimens. The figure shows that the moment degradation and rotational capacity are both affected by the b/t and h/t ratio.

Figure 9 shows the percent degradation of M_{max} (in decimal form) for the modeled sections versus the b/t (Figure 9a) and h/t (Figure 9b) ratios. The average percent degradation of M_{max} at 0.04 rad. is 16.2%, implying that some amount of buckling has occurred for most sections at 0.04 rad. Considering all 133 sections, the HSS 355.6x254.0x8.0 has the largest degradation of M_{max} at 0.04 rad. of 44.9%. Nine sections show no local buckling and do not degrade before 0.04 rad. These sections have average b/t and h/t values of 8.7 and 18.5, respectively.

The rotational capacity at $0.8M_{max}$ is plotted with respect to the b/t (Figure 9c) and h/t (Figure 9d) ratios for the 133 parametric specimens. Only eight sections do not degrade to less than 80% of the maximum moment capacity throughout the loading protocol. These sections have an average b/t and h/t ratio of 8.7 and 13.6, respectively. The HSS 406.4x203.2x8.0 shows the most severe reduction in moment capacity, reaching 80% of M_{max} at 0.022 rad. The average rotational capacity for all 133 sections is 0.045 rad. suggesting that many sections have limited local buckling and still achieve suitable behavior under large cyclic bending loads.

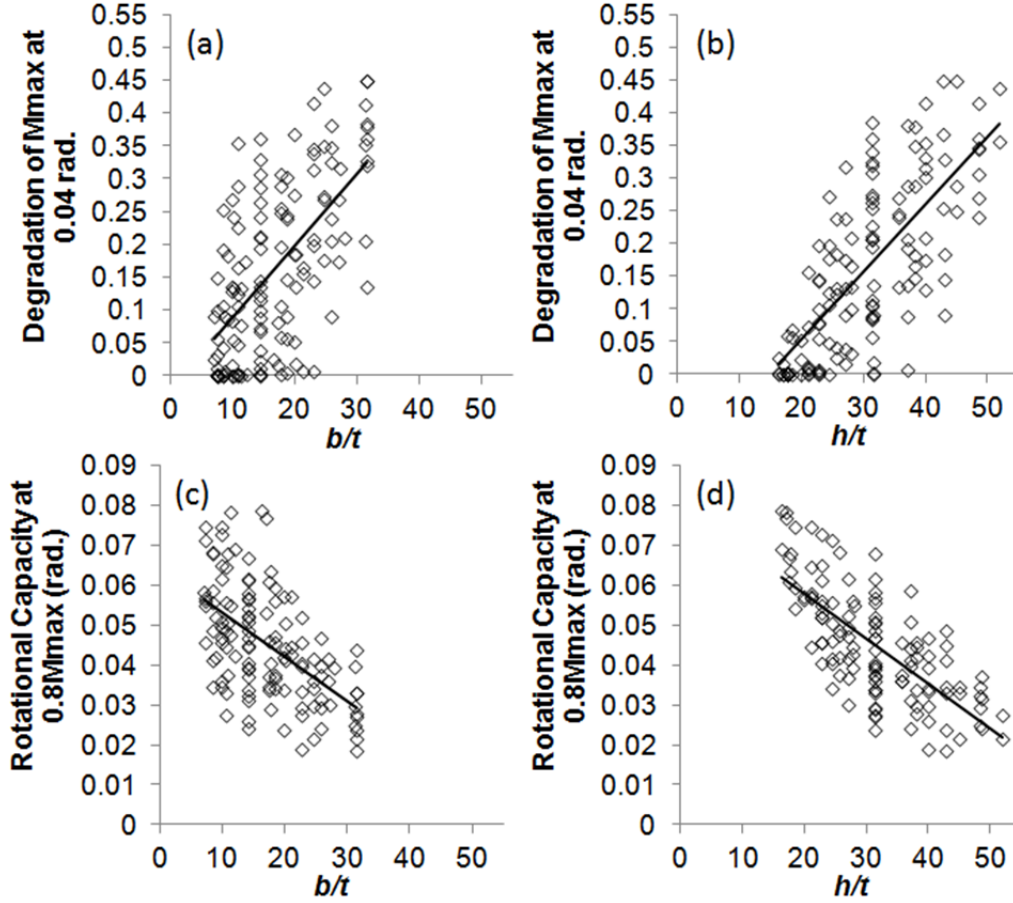


Figure 9. Degradation of M_{max} at 0.04 rad. with respect to (a) b/t and (b) h/t ; and rotational capacity with respect to (c) b/t and (d) h/t .

Linear regression lines are plotted for each graph in Figure 9. The regression lines relate the b/t and h/t ratio to the percent degradation of M_{max} at 0.04 rad. ($Deg_{0.04}$) (Eq. 1 and 2) or the rotational capacity at $0.8M_{max}$ ($\theta_{0.8M_{max}}$) (Eq. 3 and 4). When comparing the degradation of M_{max} at 0.04 rad., a change in b/t or h/t has a very similar effect with a slope of 0.011 for b/t and a slope of 0.010 for h/t . The linear regression suggests that a larger value of h/t causes less degradation in M_{max} at 0.04 rad. than the same value of b/t , implying that degradation at 0.04 rad. is often more dependent on the b/t ratio.

$$Deg_{0.04}(b/t) = 0.011(b/t) - 0.022 \quad (1)$$

$$Deg_{0.04}(h/t) = 0.010(h/t) - 0.155 \quad (2)$$

The rotational capacity at 80% of M_{max} suggests an identical dependence on the b/t and h/t ratios, since for both b/t and h/t each regression analysis slope is -0.0011. Again, the b/t ratio tends to affect the rotational capacity more than the h/t ratio because it takes a larger h/t ratio to cause the same reduction in rotational capacity.

$$\theta_{0.8M_{max}}(b/t) = -0.0011(b/t) + 0.064 \quad (3)$$

$$\theta_{0.8M_{max}}(h/t) = -0.0011(h/t) - 0.080 \quad (4)$$

This regression analysis allows for prediction of the effects of local buckling on HSS in cyclic bending for a wide range of sections. For the prediction of the degradation of M_{max} at 0.04 rad., both Equations 1 and 2 are compared for the maximum value. For most sections Equation 1 will control the degradation of M_{max} at 0.04 rad. For any section, where h/t is greater than 46.5, Equation 2 controls. When predicting the rotational capacity, Equations 3 and 4 are evaluated to find the minimum rotational capacity at which $0.8M_{max}$ is maintained. Equation 3, based on the b/t ratio, controls for most sections producing a larger reduction in rotational capacity. Only when h/t is greater than 46.1, Equation 4 controls. These relationships provide a useful connection between the geometric properties and cyclic behavior. They can be utilized as a preliminary design tool to predict the expected behavior of a section with continued cycling provided its parameter fall within the range of the parametric study.

5. Conclusions

The objective of this study was to characterize the local buckling behavior of HSS beam members under cyclic loading conditions. The local buckling behavior is correlated with the moment-rotation hysteretic behavior considering the effect of the b/t and h/t ratios. The study first utilizes eleven experimentally tested HSS beam members with b/t and h/t ratios varying from 8.46 to 31.3 and 19.9 to 48.5, respectively. Analysis of the results, based the hysteretic behavior, degradation of M_{max} at 0.04 rad., and the rotational capacity at $0.8M_{max}$, found that the b/t and h/t ratios have an effect on the local buckling behavior and that this effect is interdependent. Sections with moderate b/t and h/t ratios show local buckling in the plastic hinge region. As the b/t and h/t ratios are increased, local buckling becomes more pronounced and leads to fatigue induced fracture at the corners of the specimen.

A FEM is then calibrated to the experimental data utilizing geometric imperfections and experimentally obtained material properties. The material properties are found to vary with respect to their location along the cross-section of the HSS specimen. Material near the weld is shown to be affected by the applied heat and the corners are highly cold worked resulting in high strengths and low ductility. It is shown that using a 5.1 mm maximum imperfection for sections with b/t greater than 14.2 and h/t greater than 19.9 based on an eigenvalue buckling analysis results in a model that is able to closely match the experimental results. The model captures very similar local buckling behavior compared with that observed during experimental testing and analysis of the results correlates well with M_{max} , the degradation of M_{max} at 0.04 rad., and the rotational capacity at $0.8M_{max}$.

The FEM is also used to analyze 133 different HSS members. The parametric study moment-rotation hysteresis curves generally showed large open loops and stable, symmetric behavior. Both the b/t and h/t ratios affect the amount of inelastic local buckling. The rotational capacity at $0.8M_{max}$ for the 133 sections was compared to both the b/t and h/t ratios. The model results indicate that a change in either the b/t or h/t ratio has the same effect on the rotational capacity. Also, it should be noted that a smaller b/t ratio causes the same decrease in rotational capacity as a larger h/t ratio. Comparison of the degradation of M_{max} at 0.04 rad. shows that an increase in the b/t ratio has a slightly larger effect on the degradation of M_{max} than an increase in h/t . Linear regression analyses are provided which can be utilized to estimate the inelastic behavior of an

HSS beam member and limiting values for the b/t and h/t ratio. This will allow for use of HSS under cyclic bending loads in future structural applications.

Acknowledgments

This work is supported by the BRIGE Program of the National Science Foundation under Grant No. ECC-0926858 and the American Institute of Steel Construction through the Faculty Fellowship. The views expressed herein are solely those of the authors and do not represent the views of the supporting agencies.

References

- AISC. (2006). "Seismic design manual." American Institute of Steel Construction, Chicago, IL.
- AISC. (2010). "Manual of steel construction 14th ed." American Institute of Steel Construction, Chicago, IL.
- ASTM (2009). "ASTM E8 / E8M - 09." ASTM International, West Conshohocken, PA.
- ASTM (2011). "ASTM A370 - 11a Standard Test Methods and Definitions for Mechanical Testing of Steel Products." ASTM International, West Conshohocken, PA.
- Brescia, M., Landolfo, R., Mammana, O., Iannone, F., Piluso, V., and Rizzano, G. (2009). "Preliminary results of an experimental program on the cyclic response and rotation capacity of steel members." *Proc. STESSA 2009*, Philadelphia, PA.
- DSS (2008). "Abaqus FEA, Version 6.8-1, documentation collection." Dassault Systemes Simulia Corp., Providence, RI.
- Denavit, M. D., Hajjar, J. F., Perea, T., and Leon, R. T. (2010). "Cyclic evolution of damage and beam-column interaction strength of concrete-filled steel tube beam-columns." *Proc. 9th US National and 10th Canadian Conference on Earthquake Engineering*, Toronto, ON.
- Fadden, M and McCormick, J. (2011). "Cyclic quasi-static testing of hollow structural section beam members." *ASCE Journal of Structural Engineering* (in press).
- Goto, Y., Wang, Q.Y., and Obata, M. (1998). "FEM analysis for hysteretic behavior of thin-walled piers." *ASCE Journal of Structural Engineering*, 124(11): 1290-1301.
- Hajjar, J.F. (2000). "Concrete-filled steel tube columns under earthquake loads." *Progress in Structural Engineering and Material*, 2: 72-81.
- Hasan, S. W., and Hancock, G.J. (1988). "Plastic bending tests of cold-formed rectangular hollow sections - Research report, no R586." School of Civil and Mining Engineering, University of Sydney, Sydney, Australia.
- Key, P.W., Hasanm, S.W., & Hancock, G.J. (1988). "Column behavior of cold-formed hollow sections." *Journal of Structural Engineering*, 114(2): 390-407.
- Korol, R. M., and Hudoba, J. (1972). "Plastic behavior of hollow structural sections." *American Society of Civil Engineers Proceedings, Journal of the Structural Division*, 98(ST5): 1007-1023.
- Kurobane, Y. (2002). "Connections in tubular structures." *Progress in Structural Engineering*, 4: 35-45.
- Nakashima, M., and Liu, D. (2005). "Instability and complete failure of steel columns subjected to cyclic loading." *Journal of Engineering Mechanics*, 131(6): 559-567.
- Nishiyama, I. & Morino, S. (2004). "US-Japan cooperative earthquake research program on CFT structures: achievements on the Japanese side." *Progress in Structural Engineering and Materials*, 6: 39-55.
- Packer, J.A. (2000). "Tubular Construction." *Progress in Structural Engineering and Materials*, 2: 41-49.
- Sohal, I.S., and Chen, W.F. (1988). "Local buckling and inelastic cyclic behavior of tubular sections." *Thin-Walled Structures*, 6: 63-80.
- Wilkinson, T., and Hancock, G. J. (1998). "Tests to examine compact web slenderness of cold-formed RHS." *Journal of Structural Engineering*, 124(10): 1166-1174.
- Wilkinson, T., and Hancock, G. J. (2002). "Predicting the rotation capacity of cold-formed RHS beams using finite element analysis." *Journal of Constructional Steel Research*, 58(11): 1455-1471.